FINAL REPORT

Full Scale Measurement and Modeling of the Acoustic Response of Proud and Buried Munitions at Frequencies from 1-30 kHz

SERDP Project MR-1665

MAY 2012

Steven G. Kargl
Kevin L. Williams
University of Washington

Distribution Statement A
This document has been cleared for public release

SERDP
DOD ▪ EPA ▪ DOE

This report was prepared under contract to the Department of Defense Strategic Environmental Research and Development Program (SERDP). The publication of this report does not indicate endorsement by the Department of Defense, nor should the contents be construed as reflecting the official policy or position of the Department of Defense. Reference herein to any specific commercial product, process, or service by trade name, trademark, manufacturer, or otherwise, does not necessarily constitute or imply its endorsement, recommendation, or favoring by the Department of Defense.

Table of Contents

List of Figures ii

List of Tables iii

Acronyms iv

Abstract 1

Background 2

Materials and Methods 3

Data Processing and Discussion 7

Conclusion 20

References 22

Appendix A: PondEx09 Data Sets 24

Appendix B: PondEx10 Data Sets 25

List of Figures

Figure 1. NSWC PCD test pond and experimental configuration 3
Figure 2. Inert UXO deployed during PondEx09 5
Figure 3. Targets and rocks deployed during PondEx10 6
Figure 4. PondEx10 target field layout 6
Figure 5. Pulse-compressed baseband data and SAS images for PondEx10 targets . . . 8
Figure 6. Bistatic SAS image for targets in a 40° orientation 9
Figure 7. Pictorial description of the SAS filtering technique 10
Figure 8. Acoustic templates for 11 objects deployed in PondEx10 11
Figure 9. Finite-element meshes for bullet-shaped artillery shell 12
Figure 10. Data and hybrid model acoustic templates for aluminum replica 13
Figure 11. Data and hybrid model acoustic templates for steel replica 14
Figure 12. Scattering geometries for target-in-the-environment data/model comparison 14
Figure 13. Acoustic templates for target-in-the environment data/model comparison . . 15
Figure 14. Surface displacements for a specific elastic resonance on aluminum replica. 16
Figure 15. Acoustic templates and target strength for a nearly half-buried target 17
Figure 16. Acoustic templates for 11 objects used in PondEx10 with regions identified by a classifier as significant for classification 18
Figure 17. ROC graphs for number of feature sets sufficient for classifier training . . . 19
Figure 18. ROC graphs for different classifiers tested on the same feature sets 19

List of Tables

Table A1. PondEx09 data for a bullet-shaped steel artillery shell 23

Table A2. PondEx09 data for 81-mm mortar (filled with cement) 23

Table B1. PondEx10 data for 5 proud targets at a 10 m range 24

Table B2. PondEx10 data for 7 proud targets at a 10 m range 25

Table B3. PondEx10 data for aluminum cylinder and pipe on plexiglass plate 25

Table B4. PondEx10 data for aluminum cylinder and pipe on plexiglass plate with the plate rotated by 22° 26

Table B5. PondEx10 data for machined aluminum and steel replica on plexiglass plate 26

Table B6. PondEx10 data for a second group of 5 proud targets at a 10 m range 26

Table B7. PondEx10 data for a second group of 5 “half-buried” targets at a 10 m range 27

Table B8. PondEx10 data for a second group of 5 buried targets at a 10 m range 27

Table B9. PondEx10 data for a third group of 6 proud targets at a 10 m range 28

Table B10. PondEx10 data for a third group of 6 “half-buried” targets at a 10 m range . 28

Table B11. PondEx10 data for a third group of 6 buried targets at a 10 m range 28

Table B12. PondEx10 data for 5 proud targets at a 5 m range 29

Table B13. PondEx10 data for 5 buried targets at a 5 m range 29

Acronyms

APL-UW	Applied Physics Laboratory, University of Washington
AUC	Area under the curve
DoD	Department of Defense
FE	Finite-element
KMP	Kernel matching pursuit
LFM	Linear frequency modulated
NSWC PCD	Naval Surface Warfare Center, Panama City Division
ONR	Office of Naval Research
PCB	Pulse-compressed and baseband
PC SWAT	Personal Computer Shallow Water Acoustic Toolset
PondEx09	Pond Experiment 2009
PondEx10	Pond Experiment 2010
ROC	Receiver operating characteristic
RVM	Relevance vector machine
SAS	Synthetic aperture sonar
SVM	Support vector machine
TP	Target patch
TS	Target strength
UXO	Unexploded ordnance

Abstract

Objective: The overall objective of the conducted research is to work towards resolving issues that affect sonar detection and classification of underwater unexploded ordnance (UXO). *A central hypothesis is that the environment within which an UXO must be detected and classified significantly alters the acoustic response of an UXO and the environment must be taken into account in order to develop robust detection and classification strategies*. The primary aim is to identify and understand target and environmental factors affecting sonar performance against proud, partially buried, and buried targets and to identify robust signal features or image characteristics unique to a given UXO.

Technical Approach: Acoustic scattering from a collection of targets was collected under well-controlled and measured environmental conditions in the test pond facility at the Naval Surface Warfare Center, Panama City Division (NSWC PCD) in Panama City, Florida. The data form a database of target signatures and offer ground truth for model predictions of the acoustic scattering. The hybrid model used in our research combines a 2D finite-element (FE) model for a target response with 3D wave propagation via a Sommerfeld-Helmholtz integral. The FE model exploits the axisymmetry of the target, and each UXO has a unique FE mesh. Once the FE models are validated, environmental conditions used within the models can be altered to study changes in the acoustic scattering and to simulate environments where collection of acoustic scattering data may be infeasible due to either cost or location. Both data and model results then can be used to test current classification algorithms and provide insight into improvements of these algorithms or guidance for development of new classification schemes.

Results: The experimental data and model predictions were generated in a manner suitable for synthetic aperture sonar (SAS) processing. SAS images of individual targets and collections of targets have been constructed. In additional, a novel SAS filtering algorithm, that allows one to isolate the acoustic scattering associated with a specific target, has been applied to the data. SAS filtering was able to isolate target signatures for adjacent targets separated by ~1.5 m. The isolated target signatures are then amenable to additional signal processing techniques. Acoustic templates (also called acoustic color plots) have been generated from isolated signals. An acoustic template is a colored representation of the (absolute) target strength (TS) as a function of frequency and aspect angle. Finally, data and model predictions have been fed into a binary classifier available in the mine countermeasure community. This classifier identifies features within the data to discriminate whether a signature is UXO-like or not UXO-like.

Benefits: The research provides acoustic data on a collection of underwater targets under various environmental conditions. The data provides the ground truth in the construction of models, which then can be used to simulate the scattering responses of targets in other environments. The models can provide a cost savings by reducing the number and/or duration of field tests. By providing a capability to simulate sonar performance, the Department of Defense can make informed decisions on the relative merits of existing sonar systems and on proposed modifications to these systems for underwater UXO management. Finally, other researchers can leverage the data and analysis techniques developed under SERDP project MR-1665.

Background

Although the practice of disposing conventional and chemical munitions in coastal waters was discontinued during the 1970's, the environmental, economical, and even the recreational impact persists [1]. In Overfield and Symons' overview of the Resources and Undersea Threats (RUST) database, they note that over 2100 underwater sites are likely to contain shipwrecks, munitions dumpsites, and radiological waste as well as abandoned pipelines and wellheads [2]. Of those 2100 sites, verification has been completed on only slightly more than 50% with contemporary records (i.e., not through physical survey or assessment). Although not all sites listed in the RUST database contain discarded munitions, the database also may not contain a comprehensive list of current and former DoD training facilities. In any event, there is a clear need for cost-effective physical surveys of possible underwater munitions sites. Schwartz and Brandenburg summarize the current technologies available for underwater UXO applications [3]. Their Table 1 includes metal detection (e.g., magnetometers and electromagnetic induction), chemical sensors (e.g., spectroscopy and fluorescence), and sonar. Metal detection and chemical sensors are typically restricted to short ranges; while the sonar technologies considered are limited in range (e.g., Didson system) or are limited by poor penetration into sediments due to the high frequencies used (e.g., side-scan sonar). Furthermore, Schwartz and Brandenburg note that SAS is still a relatively new technology in UXO detection and that low-frequency SAS systems have demonstrated detection of proud and partially buried objects [4].

Low-frequency SAS systems with a wide bandwidth have several advantages over higher frequency sonar systems. Low frequencies offer greater detection ranges, which permits the rapid surveying of wider areas. In addition, low frequencies attain greater penetration depths into sediments, which permit detection of partially and completely buried munitions. The range resolution of a SAS system is related to the bandwidth of the transmitted signal where a wider bandwidth provides higher resolution. Thus, we report here our research on UXO detection and discrimination by a low-frequency wide-bandwidth SAS system.

Our work compliments that of Bucaro *et al* in that they consider isolated UXO in their research [4]. Our quick-look experiments conducted during Pond Experiment 2009 (PondEx09) deployed isolated targets; while the experiments during Pond Experiment 2010 (PondEx10) had multiple objects in the field of view of the SAS system with a minimum separation distance approaching ~1.5 m. Acoustic scattering from two inert UXO in an underwater environment were collected during a one week extension of PondEx09 from 13 Feb 09 through 18 Feb 09. These two UXO were again deployed during PondEx10 along with an additional nine targets, and data were collected over a three week period from 06 Mar 10 through 25 Mar 10. This report describes the experiments, the acoustic scattering data, data processing techniques, and compares hybrid model predictions to the experimentally measured data.

Objective:

The results of this research can be incorporated into sonar simulation software such as PC SWAT from NSWC PCD and can be used to develop and test computer-aided detection and classification software for sonar designed to search for UXO. Additional factors that need continued study are gas content in muddy sediments, sediment attenuation and dispersion, sediment heterogeneity, sources of variation in target acoustic response (e.g., target or

environment induced), and how variations in the acoustic response of a given target affect classification. Our goal is to assess the significance of these factors by exercising quantitatively predictive scattering models including these factors and comparing the predictions to well-controlled test pond measurements.

A series of monostatic and bistatic acoustic scattering measurements were conducted to investigate discrimination and classification capabilities based on the acoustic response of targets for underwater unexploded ordnance (UXO) applications. The measurements utilized a rail system with a mobile sonar tower and a stationary sonar tower. Each tower is instrumented with receivers while the sources are located only on the mobile tower. For PondEx10, eleven targets were deployed at two distinct horizontal ranges from the mobile tower system. Acoustic data were initially processed using synthetic aperture sonar (SAS) techniques, and the data were further processed to generate acoustic templates for the target strength as a function of frequency and aspect angle. Results of the processing of data collected from targets are presented. Also presented are the results associated with a processing technique that permits isolation of the response of an individual target, which is in close proximity to other targets.

Materials and Methods

Test Pond Facility

PondEx09 and PondEx10 were conducted at NSWC PCD's facility 383, which contains a fresh water pond. This pond holds approximately 9 million gallons of water with dimensions of ~110 m in length and ~80 m in width at its surface. The water depth at the location of the deployed target fields is ~14 m. The bottom of the pond is covered with a ~1.5 m thick layer of medium-fine sand. To prevent biological growth and fouling of the targets and equipment, the water is filtered and chlorinated. During the measurements, temperature readings from the divers' dive computers were used to estimate the sound speed of the water. For PondEx09 and PondEx10, the sound speeds were 1448 and 1456 m/s, respectively. Figure 1 shows an aerial view and engineering drawings of the pond, which depict APL-UW's rail and location(s) of the target(s) with respect to the rail.

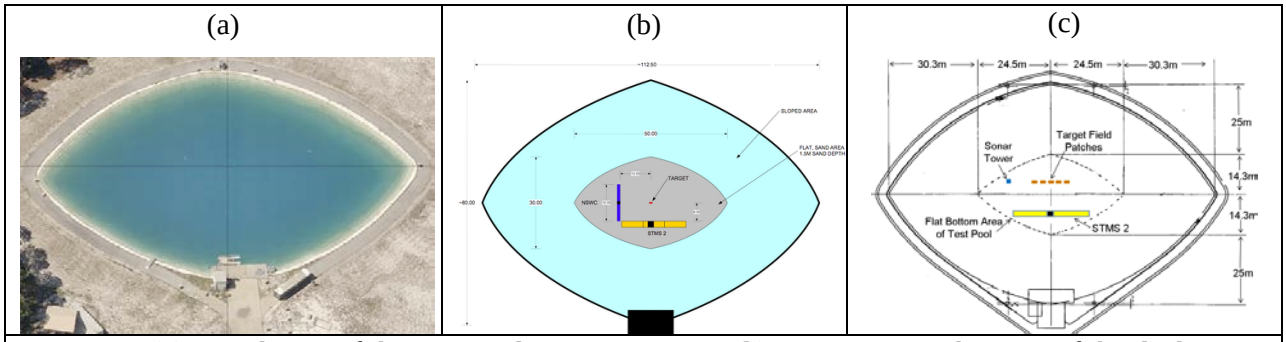

Figure 1. (a) Aerial view of the test pond at NSWC PCD. (b) Engineering schematic of the deployment of the APL-UW rail (gold) and NSWC PCD rail (blue) during PondEx09 and the target location within the target field. (c) Engineering schematic of the deployment of the APL-UW rail (yellow) and NSWC PCD sonar tower (blue) during PondEx10 and five target patches within the target field.

Pond Experiment 2009

A top view of the PondEx09 measurement field is depicted in Figure 1(b). Two rail systems were deployed orthogonal to each other (blue and gold bars). Each rail included a mobile tower that could be positioned anywhere along its rail or moved continuously down the rail while transmitting short pulses. An acoustic source and receiving array were mounted on APL-UW's mobile tower (black box), which could move along the rail designated as STMS-2 (gold bar) in Figure 1(b). The source and receiver heights above the mean water-sand sediment interface were 3.73 and 3.96 m, respectively. The effective aperture of the source was 0.3×0.3 m^2. The receiving array contained 6 channels where the horizontal aperture for each channel is 0.1 m, and the 6 vertical apertures are 0.3, 0.1, 0.1, 0.1, 0.1, and 0.3 m from channel 7 (top array element) to channel 12 (bottom array element), respectively. (The channel number corresponds to the pre-amplifier number.) The source and receiver were rotated to a 40° depression angle, so the acoustic axis of each intersected the sediment at a horizontal range of 5 m. For a SAS data set, the tower was scanned along the STMS-2 rail at 0.05 m/s, and the source transmitted and the receiver collected data at a 2 Hz repetition rate. Thus, a spatial increment of 0.025 m was achieved between adjacent signals, and each signal was recorded for 30 ms. During data collection, the tower is automatically stopped by limit switches at the ends of the rail. To ensure a complete set of signals are collected the source transmitted more chirps than actually required. Thus, a set of data contains 800 signals, where only 750 signals typically are used in the data analysis. A complete SAS data set of 750 signals has a physical SAS aperture of 18.75 m.

During the collection of the SAS data, NSWC PCD positioned a receiver (black box) at a horizontal location of 5 m along the NSWC rail (blue bar) in Figure 1(b). The nominal receiver height was 4 m above the mean sediment interface. In this manner, a bistatic SAS data set was collected simultaneously with the APL-UW SAS data. An additional bistatic SAS measurement was collected, where the APL-UW tower was placed at the center of the STMS-2 rail. The source transmitted a sequence of pulses at a 2 Hz repetition rate, and the NSWC PCD tower was positioned at various locations along the NSWC PCD rail. At each position, 10 received signals were averaged to improve the signal-to-noise ratio.

Two linear-frequency-modulated (LFM) chirps were used throughout the experiments on two inert UXO. When the APL-UW tower traveled from left-to-right in Figure 1(b), a chirp with a 6 ms duration, 16 kHz carrier frequency and 30 kHz of bandwidth was transmitted. During the return travel, a 4 ms duration chirp with a 40 kHz carrier frequency and 20 kHz of bandwidth was transmitted. Although the 30-50 kHz chirp exceeds the frequency range of the proposed research, it was desirable to collect the 1-31 kHz data with the tower always moving in the same direction. Thus, the return travel of the tower along the rail provided an opportunity to collect additional data that may impact the detection and classification of underwater UXO. It is also noted that the aperture of the 30-50 kHz source is $l\times w = 0.1\times0.05$ m^2, where l is horizontal length and w is vertical width.

Figure 2 displays the two inert UXO used in the collection of the PondEx09 data. In the left panel, the bullet-shaped artillery shell is a solid steel projectile with a 4.2-inch diameter. In the right panel, the UXO is an 81-mm mortar filled with an inert material. The yellow line above the

mortar is attached at the center of the STMS-2 rail, and stretched perpendicularly across the target field by divers during manipulation of the target. The black tie-wrap, visible in Figure 2, marks a 5 m horizontal range from the STMS-2 rail. As shown, the mortar is in a broadside orientation with respect to the rail, i.e., the cylindrical axis of symmetry of the mortar is parallel to the path of the SAS platform. Finally, during data collection the line is withdrawn from the target field and placed beneath the rail.

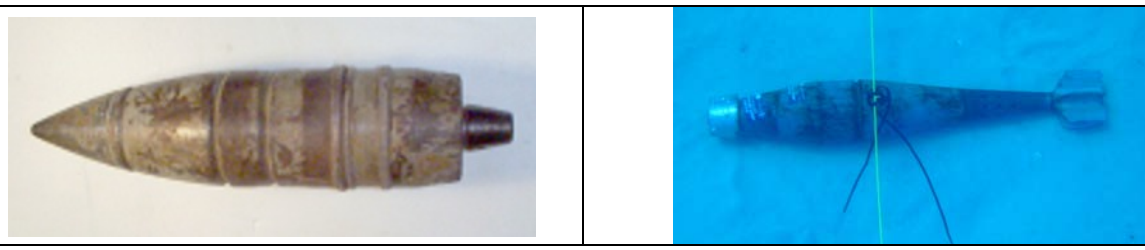

Figure 2. *Left: bullet-shaped steel artillery shell. Right: 81-mm mortar in a broadside orientation to the APL-UW rail. The yellow line and attached black tie-wrap permit rapid placement of the UXO in the center of the target field.*

With a UXO at a 5 m horizontal range and centered along the APL-UW rail, the maximum possible angular span in a single measurement is $\tan^{-1}(\pm 9.375/5) \approx \pm 62°$. The beam patterns of the source and receiving array further reduce the angular span; hence, to cover the full range of aspect angles for the target scattering, the target was placed at various orientations in the target field. The orientations, data sequence numbers, burial state of the UXO, and frequency band of the LFM chirp are listed in Tables A1 and A2 in Appendix A. In the 0° orientation, the nose of the UXO is pointed at the APL-UW rail and it is broadside to the NSWC PCD rail. At 90°, the UXO is broadside to the APL-UW rail and the nose is pointed towards the NSWC PCD rail. When the target is rotated to 180°, its tail is pointed at the APL-UW, and it is again in a broadside orientation to the NSWC PCD rail. The UXO is rotated clockwise by a 20° increment. This ensures an overlap of the angular ranges from adjacent rotations, which facilitates alignment of the acoustic templates (i.e., the target strength as a function of aspect angle and frequency) generated from the data.

Pond Experiment 2010

Eleven targets were deployed in the measurements. The targets included a solid aluminum cylinder, an aluminum pipe, an inert 81-mm mortar filled with an inert material, a solid steel artillery shell, two machined aluminum replicas of the bullet-shaped artillery shell, a machined steel replica of the bullet-shaped artillery, a de-militarized 152-mm TP-T round, a de-militarized 155-mm empty howitzer projectile without a fuse or a lifting eye, a small aluminum cylinder with a notch, and two rocks. As can be seen in Figure 3, the sizes of the rocks are comparable to other targets. Figure 3 shows all of the targets except the solid aluminum cylinder. The machined aluminum and steel replicas were constructed from materials with known properties and are based on a CAD drawing of the bullet-shaped steel artillery shell. The solid aluminum cylinder is 2 ft long with a 1 ft diameter and was deployed as a reference target during PondEx09 and PondEx10. The aluminum pipe is 2 ft long with an inner diameter of 1 ft and 3/8 inch wall thickness. For convenience the cylinder and pipe are referred to by their aspect ratio defined by the length:diameter, e.g., 2:1 aluminum pipe.

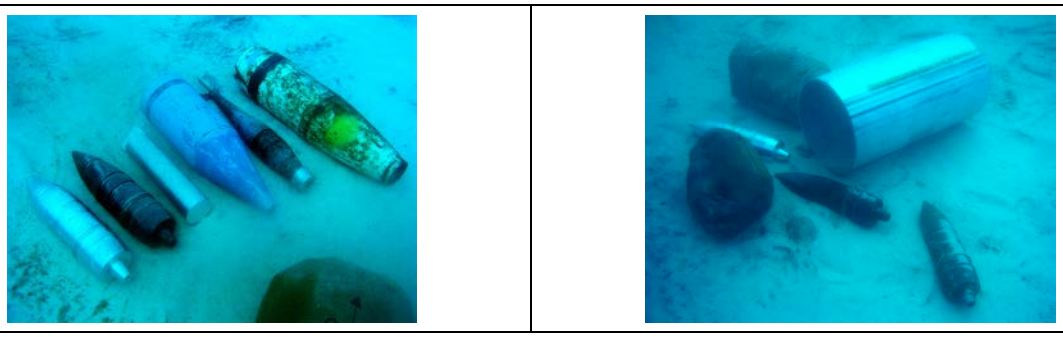

Figure 3. Underwater images of several targets used during PondEx10. In the left panel, the blue target is a 152-mm TP-T round and the target with the yellow marking is a 155-mm howitzer projectile.

A rough layout of the 10 m target field is illustrated in Figure 4. Divers first deployed the 21 m long APL-UW rail system, which consists of three independent sections (see Figure 1 in [5]). The sections are connected and leveled to establish a baseline for the geometry of the experiment. The divers then surveyed in two screw anchors at an 11 m horizontal range from the rail. This task is accomplished by using two temporary lines attached at the ends of the rail and forming a right triangle to locate A and B. A lightweight guide line is then stretched between the screw anchors and marked at 4, 7, 10, 13, and 16 m from the left screw anchor. These locations are enumerated and mark the sites of 1 m^2 diver-flattened patches, where targets are deployed (dark blue patches in Figure 4). For brevity, Target Patch numbering will be abbreviated to, for example, TP1. When more than five targets are placed into the field, the additional targets are put in the 1 m^2 patches between TP2 and TP3 and TP3 and TP4 (light blue patches in Figure 4).

Figure 4. Schematic layout of the PondEx10 target field. Screw anchors are located at A and B, and mark the end of a light weight guideline, which is parallel to the rail. The numbered blue squares are sites of diver flattened patches for the initial set of experiments; while the light blue patches were used in later measurements.

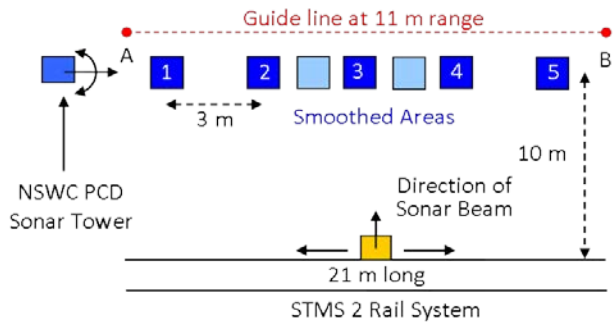

Target patches were created by the divers using a set of T-bar aluminum rails that are registered against the 11 m guide line. The T-bar aluminum rails are set perpendicular to the guide line, separated by ~1 m, and then driven into the sand. The rails are checked for level and adjusted as needed. Divers smoothed the water-sand interface by scraping a third aluminum bar along these rails. This bar is held perpendicular to the two T-bar rails. Low spots are filled with sand from outside the target field, and excess sand accumulates near the front and back of the target patch. The excess sand is hand-smoothed to prevent the build up of a small berm. This procedure is followed prior to a set of measurements, where a set is defined by a number of target rotations relative to mobile-tower/rail system.

To orient the targets, a square PVC frame with dimensions slightly larger than the target patch is utilized. One side of the frame is referenced to the 11 m guide line. A series of holes in the frame allowed the divers to select one of several angles. The angles used in PondEx10 for

targets with cylindrical symmetry ranged from −80° to 80° in 20° increments. A target is broadside to the rail system at 0° with the nose of a UXO pointing towards the stationary tower. The nose (tail) of a UXO pointed towards the rail in the −80° (80°) orientation. For the rocks, the rotations covered −80° to 280° due to their asymmetry.

The mobile tower is placed on the rail system, and it holds acoustic sources and receivers. The mobile tower moves at 0.05 m/s with the source transmitting a ping every 0.5 s. The total distance traveled along the rail is 18.75 m. A SAS data set contains 750 pings, and each data set is referred to by a "sequence number". The receiver on the mobile tower is a six channel vertical array and each channel is recorded separately at a 1 MHz sample rate. The acoustic receivers located on the stationary sonar tower (see Figure 4) were mounted on horizontal pan and vertical tilt motors. This allowed accurate alignment of the main lobe of the receivers with the target patches. The stationary receivers recorded data at a 500 kHz sample rate. The sources and receivers on both the rail system and stationary sonar tower stood about 4 m above the water-sand interface. When traveling from left-to-right in Figure 4, a source transmitted a 6 ms LFM chirp centered at 16 kHz with 30 kHz of bandwidth. On the return trip, a second source transmitted a 4 ms LFM chirp centered at 40 kHz with 20 kHz of bandwidth.

Two target fields were deployed during PondEx10: one with targets at a 10 m horizontal range from the rail system and one with targets at a 5 m horizontal range. At a 10 m range, the targets were proud on a flattened water-sand sediment interface or partially buried to nearly half their diameter. Data were also collected for buried targets at a 10 m, but those data were not used in the research reported here. The targets were either proud, half-buried, or flush buried when placed at 5 m. The 10 and 5 m ranges correspond to ~20° and ~40° grazing angles with respect to the source and receiver locations, respectively. The critical grazing angle for the sand in the test pond was nominally 28°. Thus, data collected for the proud and "half-buried" targets were at shallow and steep grazing angles; while data collected for the fully buried targets corresponded to a steep grazing angle case only. When five targets were placed in the target field, the separation distance between adjacent targets was approximately 3 m. This distance was selected to minimize multiple scattering between targets. When the additional two targets were inserted into the target field, the separation distance was reduced to 1.5 m for the inner five targets. The data sets collected during PondEx10 are tabulated in Appendix B.

Data Processing and Discussion

SAS Imaging and Acoustic Templates

The data were initially processed using time-domain and frequency-domain synthetic aperture sonar (SAS) techniques in which high resolution images were generated. A brief description of the time-domain method is given in [6]. First, a SAS data set is pulse compressed by match filtering the pings with a replica of the transmitted LFM chirp. During the match filtering, a Hilbert transform converts the real-valued recorded pings to complex-valued signals. Pulse-compressed baseband (PCB) data are then obtained by multiplying by $\exp(i\omega_0 t)$, where ω_0 is an angular carrier frequency and our processing scheme assumes a negative time convention. The left-hand-side of Figure 5 shows the magnitude of the PCB pings for sequences 253, 255, 257, 259, and 261, where the transmitted signal was the 1-31 kHz LFM chirp. The corresponding SAS images generated from the PCB data are displayed in the right-hand-side of Figure 5. For

these sequences, the targets were placed proud on the water-sediment interface at a 10-m range from the APL-UW rail system. The targets included a 152-mm TP-T round (top), small aluminum cylinder with a notch, real steel artillery, an aluminum replica of the bullet-shaped artillery shell, 81-mm mortar filled with cement, and an empty 155-mm howitzer shell (bottom). These targets are shown in the left panel of Figure 3. Figure 5 depicts 5 of the 9 orientations of the targets with respect to the APL-UW rail system listed in Table B9.

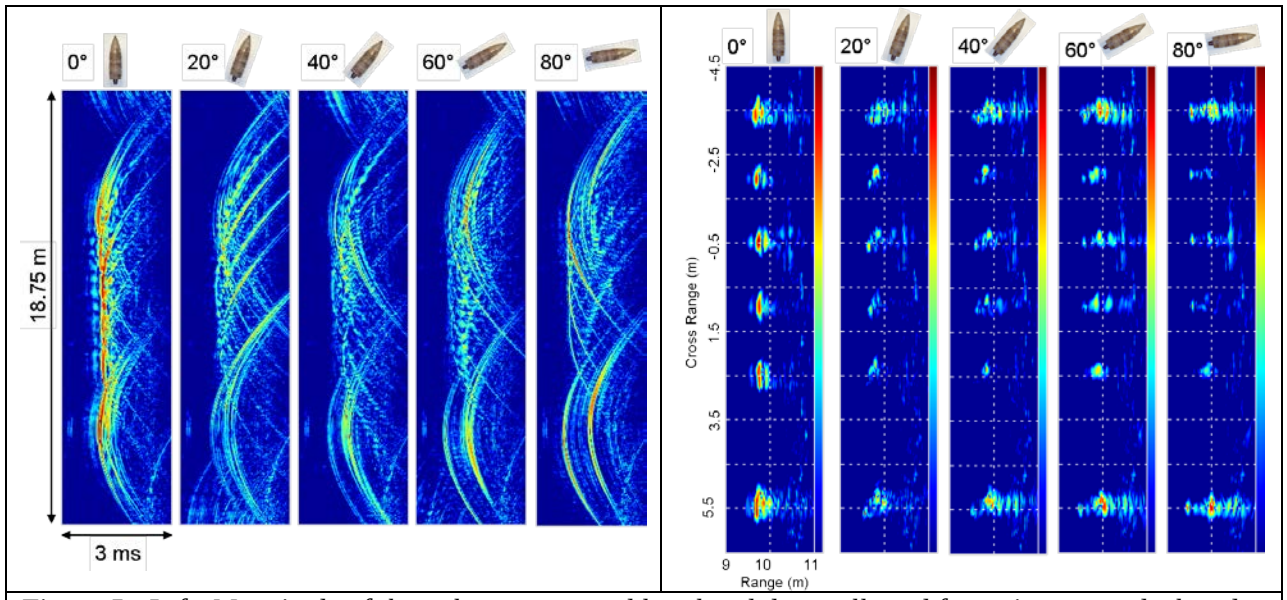

Figure 5. Left: Magnitude of the pulse-compressed baseband data collected from six targets deployed at a 10 m range in the target field. The time duration for each panel is 3 ms, and a data set contained 750 pings, which gave a SAS aperture of 18.75 m. Right: SAS images created from the PCB data. The orientation of the targets is depicted above each panel, and the rotation angle is referenced to a straight-line path of the SAS platform (i.e., the APL-UW rail system). The rotation is in the image plane. For the SAS processing, the width of the image was selected to be 2 m.

It is immediately evident that the scattered acoustic field from an individual target interferes with its neighbors. The overlap of the scattered acoustic fields has an important consequence for the acoustic template processing. However, for SAS processing the coherent addition of the complex time signals is unaffected by this overlap. To produce a SAS image, the time-domain data is processed with a simple delay-and-sum beamformer. For each pixel in a SAS image, the signals are time-shifted to account for propagation delays from the source to the pixel and then from the pixel to the receiver. Once the time shift is performed, the signals are coherently added to determine a complex reflectivity for the pixel. This time shifting is done for each pixel in a SAS image. The color bar is a relative dB scale (red is 0 dB and blue is −25 dB), which is determined from the magnitude of the "loudest" pixel with the two-way geometric spreading loss removed. Finally, images for individual channels of the receive array as well as the superposition of the six channels have been constructed. The procedures to produce PCB data sets and SAS images were applied to all sequences given in Appendix B, and reported in the second interim report for SERDP project MR-1665.

Figure 6, generated from sequence 258, is an example of the bistatic images generated by processing data using the time-domain SAS methods. The source on APL-UW's mobile tower

transmitted an acoustic signal, which was a 4 ms LFM chirp with a 40 kHz carrier frequency and 20 kHz bandwidth. While it traveled the length of the rail, a receiver on NSWC PCD's stationary tower recorded the scattered signals. The targets were all in a proud configuration oriented at 40° (see Figure 5 above). Figure 6reveals a target separation for the first five targets (from left to right) was ~1.5 m corresponding to the minimum separation distance examined during PondEx10; while the far-right target had a separation distance of ~3 m from the fifth target. In this image the color scale corresponds to a logarithmic scaling of the scattered intensity relative to the image maximum over a 30 dB range. Inspection of Figure 6 shows a reduction in the background reverberation, because the receiver is not within the acoustic field scattered by the water-sediment interface in the forward direction. Additional, bistatic results are discussed in [6] and [14].

Figure 6. Bistatic SAS image of the targets discussed in Figure 5. Both the orientation of the targets within the target field and the separation distance between adjacent targets agree with diver measurements.

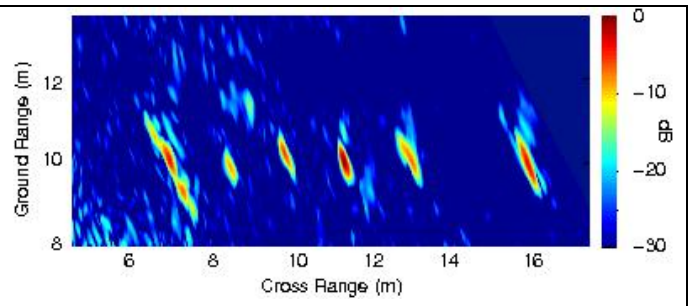

The SAS data were further processed to generate acoustic templates of the target strength as a function of frequency and aspect angle. Due to the relatively small separation distances between the targets, the scattered acoustic fields from the targets overlap as is evident in Figure 5. To generate an acoustic template, a SAS filtering technique was used to isolate the response of individual targets and to suppress reverberation noise. A detailed description of the filtering technique has been given by Marston et al [7]. A pictorial description of this technique is shown in Figure 7 and a brief summary is as follows. The raw SAS data set is deconvolved with a target arc for a single selected location in an image plane, and a SAS image is formed. Marston et al implemented a frequency-domain SAS imaging algorithm, which is known as an ω-k SAS algorithm [8]. As an observation point in the SAS image moves away from the selected location, the image becomes defocused because the target arc is not appropriate for these locations. The SAS image is then windowed in the spatial domain about the selected location. This windowed SAS image contains the information to reconstruct the time signals associated with a given target via a convolution with the same target arc. It is noteworthy that the deconvolution and convolution processes are linear operations, and hence in the absence of multiple scattering the recovered signal isolates the response of the selected target. We have applied this algorithm to our monostatic data and have generated acoustic templates for the 11 targets deployed during PondEx10. A SAS filtering algorithm appropriate for a bistatic source/receiver configuration was unavailable at the time data were being processed, so the bistatic SAS data were not used in the generation of acoustic templates due to the overlapping target signals.

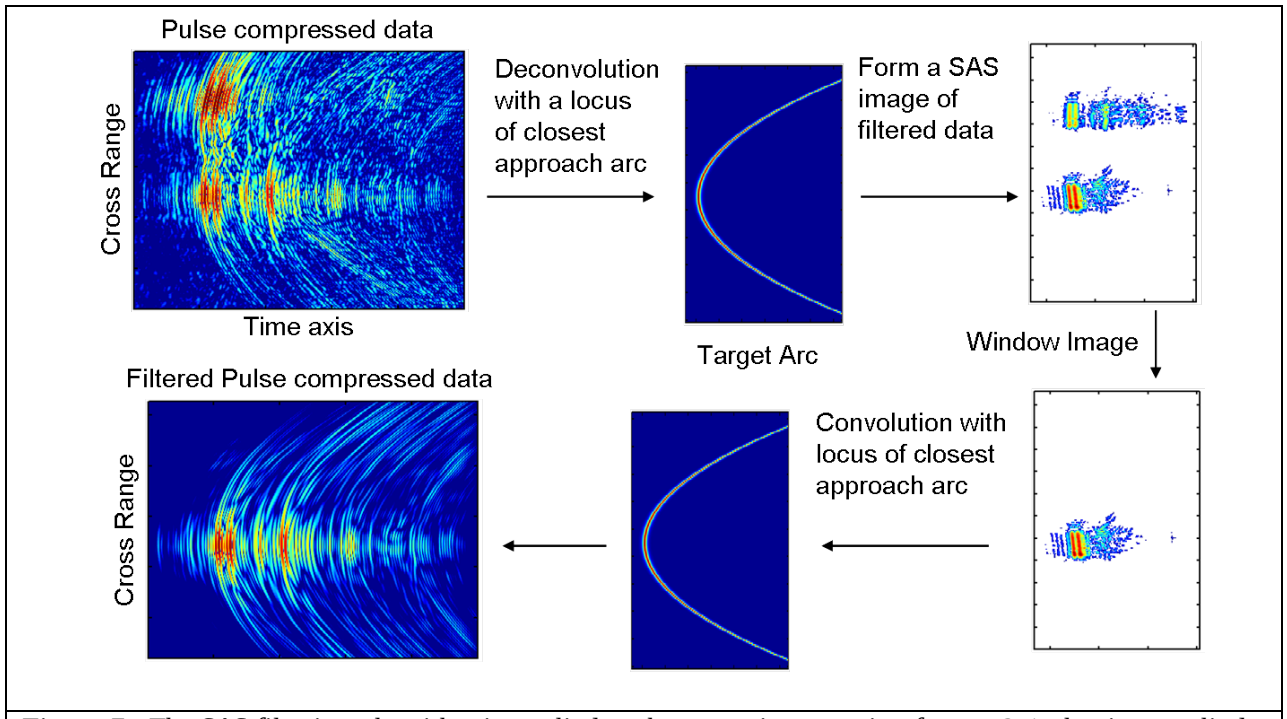

Figure 7. The SAS filtering algorithm is applied to the acoustic scattering from a 2:1 aluminum cylinder (lower target) and a 2:1 aluminum pipe (upper target). The top row depicts the deconvolution of a target arc located at the aluminum cylinder. The lower row depicts the spatial windowing and convolution with the same target arc to recover the scattering from the cylinder. The final PCB data not only contains only the cylinder response but it is clear that noise associated with surface reverberation has been suppressed.

Inspection of the PCB data in the left panel of Figure 5 suggests that, at most, an aspect angle range for a given target at a 10 m range in a given sequence spans approximately ±15°. This motivated the choice of target rotations from −80° to 80° in 20° increments for the axisymmetric targets. Adjacent rotation angles provide an overlap in the aspect angle ranges (e.g., 20°±15° and 40°±15°), which permits the nine sequences to be stitched together to form an acoustic template. The overlapping regions can be determined by a cross-correlation of the aspect angle ranges for adjacent rotation angles or aligned by eye (given sufficient structure in the color plots). Once the overlap is established, the two angular ranges are merged by a smoothing operation over the overlap region. Acoustic templates for the 11 PondEx10 objects are shown in Figure 8.

Comparisons of the acoustic templates in Figure 8 suggest that an acoustic template may be used as a fingerprint to uniquely identify a given target. The use of these acoustic templates with a binary classifier is discussed below. It is, however, noteworthy that the acoustic templates in Figure 8 were collected at a single freshwater location under fairly well-controlled and well-measured environmental conditions. Whether observable structure in an acoustic template is robust under variations in the acoustical properties of the environment remains to be established. For example, PondEx09 and PondEx10 data were collected in late-winter and early-spring time frames, when the freshwater had a nominal sound speed of ~1450 m/s. Under summer conditions the speed of sound in freshwater can exceed 1500 m/s and in sea water it can exceed 1530 m/s. In addition, the current research has been performed with a sand sediment, the

robustness of the acoustic templates also needs to be established for changes in sediment type (e.g., mud typically has a lower sound speed than the overlying water). Finally, the robustness of an acoustic template for a target needs to be examined in the presences of surrounding clutter. Our initial effort with target classification, discussed below, suggests that acoustic templates may be useful in target classification schemes, but additional research is needed to improve the rejection of clutter.

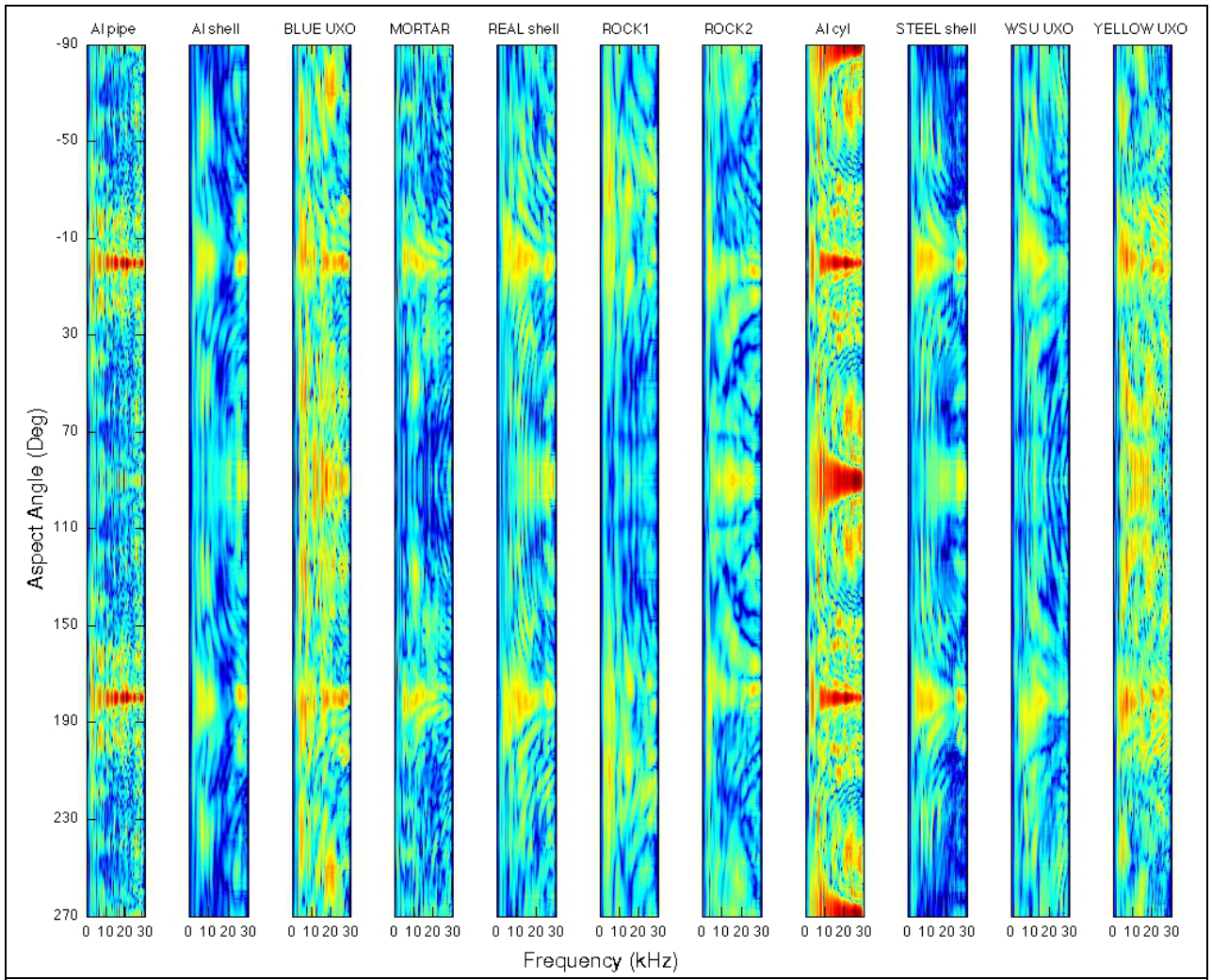

Figure 8. Acoustic templates for the collection of PondEx10 targets. The 152-mm TP-T and 155-mm howitzer projectile are labeled the "BLUE UXO" and "YELLOW UXO. The bullet-shaped artillery shell and the aluminum and steel replicas are labeled "REAL shell", "Al shell", and "STEEL shell", respectively. The 2:1 aluminum pipe and solid cylinders are "Al pipe" and "Al cyl," and the acoustic template labeled "WSU UXO" is the small aluminum cylinder with a notch.

Finite-element Models and Comparison to Data

The experimental acoustic templates in Figure 8 serve as ground truth for acoustic templates generated from predictions of the target responses from a hybrid model. Our hybrid model combines N×2D FE models, which solve the 3D problem of the interaction of an acoustic field with a target in terms of a superposition of N azimuthal Fourier modes, with a 3D Helmholtz-

Kirchoff propagation integral. The targets are axisymmetric, but the incident field is generally not axisymmetric. The N×2D FE method allows us to solve problems over the entire frequency bandwidth without resorting to supercomputers. Details of the underlying assumptions and implementation are contained in [9], [10], and [11].

One of the first questions to address is: "What level of detail is needed in a FE model to reproduce the observed structure in an experimental acoustic template?" FE meshes for the bullet-shaped artillery shell (and its replicas) were constructed with and without the grooves and ridges on its surface. The material properties of the actual steel used in the artillery shell are unknown, so the FE models are executed with the properties of aluminum to compare with the template labeled Al shell in Figure 8. The density, compressional sound speed, and shear sound speed for aluminum are ρ = 2700 kg/m^3, c_l = 6568 m/s, and c_s = 3149 m/s, respectively. The meshes are depicted in Figure 9. The smoothed mesh contains 3533 elements and 24526 degrees of freedom (DOF). The mesh with grooves and ridges contains 9608 elements and 77233 DOF. The fine-grain sand sediment was treated as a viscous fluid with density and complex sound speed of ρ_1 = 2000 kg /m^3 and c_1 = 1694 + i1.355.

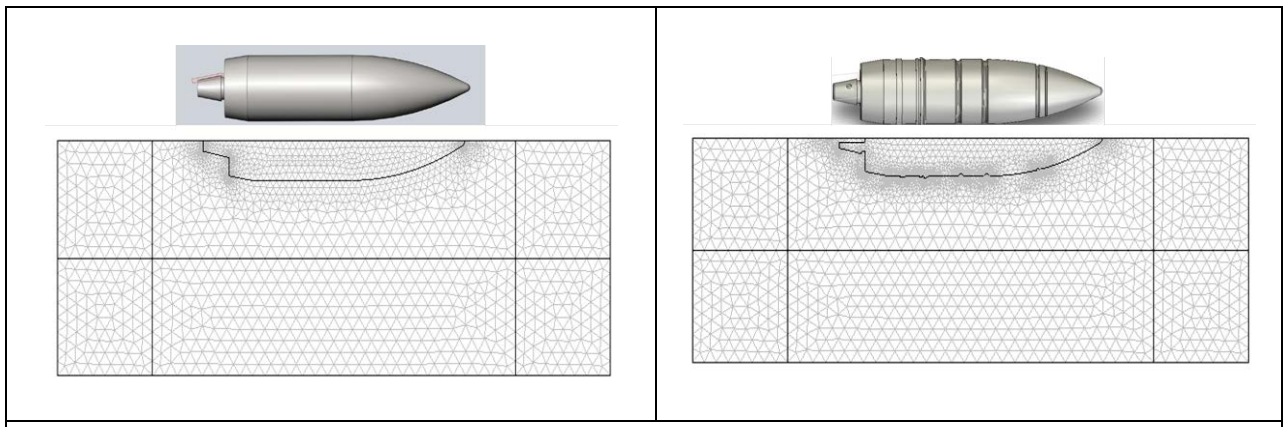

Figure 9. Left: Mesh for a smoothed UXO. Right: Mesh for an UXO with grooves and ridges. The fine structure on the surface is the site of a concentration of elements. This then leads to an increase in computational complexity.

The predicted acoustic templates and the acoustic template generated from PondEx10 data are shown in Figure 10 for the Al shell on a water-sand sediment interface. At low frequencies, both FE meshes capture the elastic response of the aluminum replica shell, but as the frequency increases one sees that the grooves and ridges must be included in the FE model to recover the observed structure. The highest frequency in the experiments and simulations is 30 kHz, and with a nominal sound speed in water of 1464 m/s the wavelength is ~4.9 cm. The depth, height, and width of the grooves and ridges are on the order of a few millimeters. The separation distances between adjacent surface features are on the order of a wavelength. Hence, it seems that the propagation of acoustic energy along the surface is affected by the spacing of the surface features, and this gives rise to some of the observed differences in the acoustic templates of Figure 10.

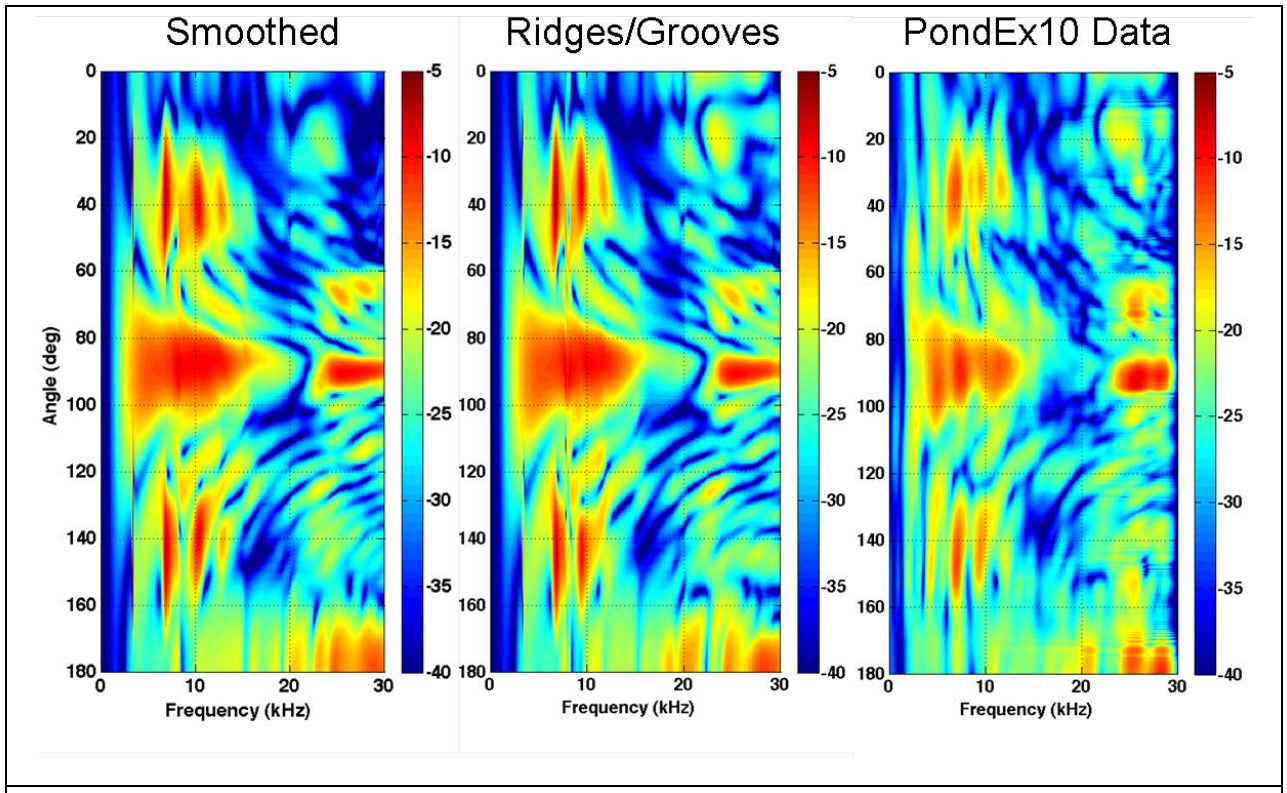

Figure 10. Acoustic templates for the smoothed FE mesh simulation (left), FE mesh with grooves and ridges simulation (center), and the PondEx10 data for the bullet-shaped artillery shell (right). Agreement is satisfactory at low frequency, but as the frequency increases above 15 kHz the simulation with the ridges and grooves captures structure observed in the data.

With the required FE mesh fidelity established, the material properties of the steel replica were used to compute an acoustic template. The material properties for the mild steel, used in the construction of the steel replica, are ρ = 7710 kg/m^3, c_l = 5890 m/s, and c_s = 3240 m/s. The hybrid model was exercised with the FE mesh containing grooves and ridge, and the results are shown in Figure 11. Comparison of the hybrid model results with the PondEx10 data immediately shows that the steel replica result is in much better agreement than aluminum replica result. Given that the targets are geometrically identical, it is the elastic response of the targets (i.e., the material properties) that gives rise to observed agreement. It is, however, noteworthy that the steel replica result and PondEx10 data do show some distinct disagreement. This can be attributed to a mismatch in material of the steel of the actual UXO and mild steel. In addition, the hybrid model simulation does not include noise contributions for surface reverberation whereas the PondEx10 data contained some reverberation even though the divers had artificially smoothed the water-sediment interface.

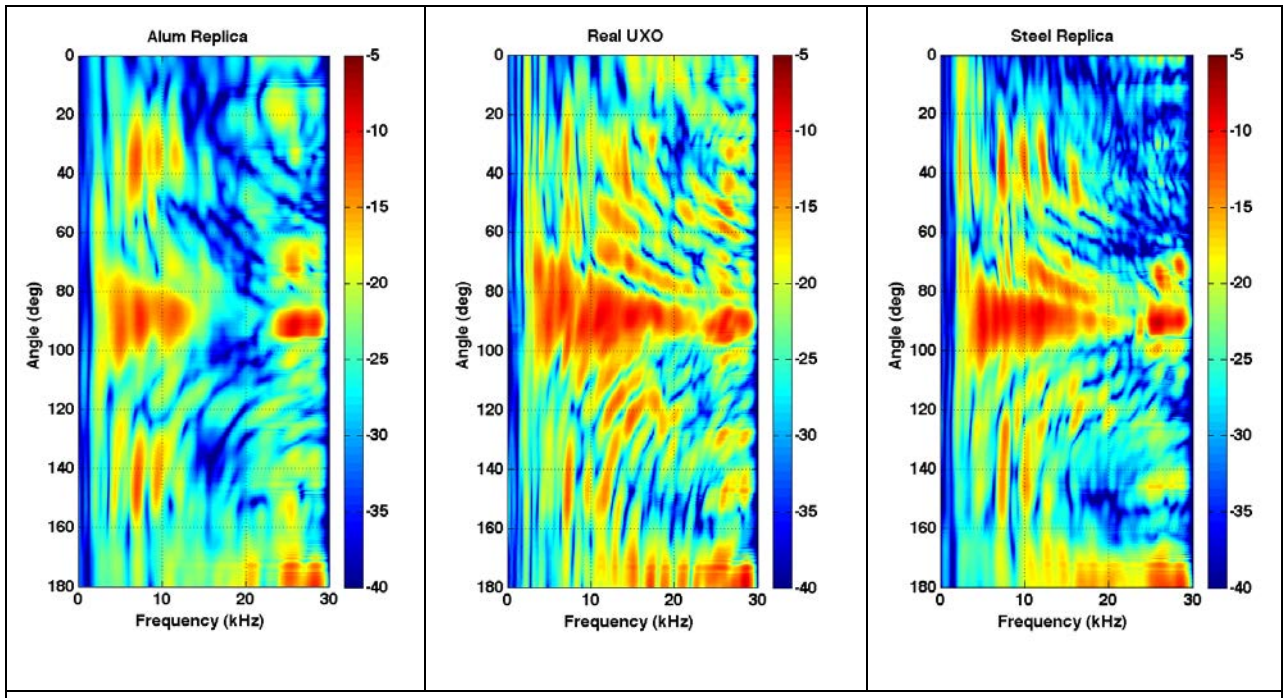

Figure 11. Acoustic templates for the aluminum replica (left), real steel artillery shell (center), and steel replica (right). The hybrid model was executed with an FE mesh with grooves and ridges. The FE model results do not include noise contributions from surface reverberation.

Figures 10 and 11 suggest that an acoustic template can be used as a fingerprint for an UXO. But, the response of a target may be affected by the environment and the scattering geometry within that environment. To investigate the robustness of the observed structure in the acoustic templates, we analyzed the acoustic scattering from an aluminum replica under three scenarios, where the scattering geometries are shown in Figure 12. The local grazing angle for the 10 m horizontal range is ~21° and it is well below the critical grazing angle for total internal reflection from the sediment. The critical grazing is ~28°. Figures 12(b) and 12(c) depict the target at a 5 m horizontal range, which corresponds to a grazing angle of ~38°. For the buried target case, this means that the acoustic energy arrives at the target via ordinary refraction as governed by Snell's law.

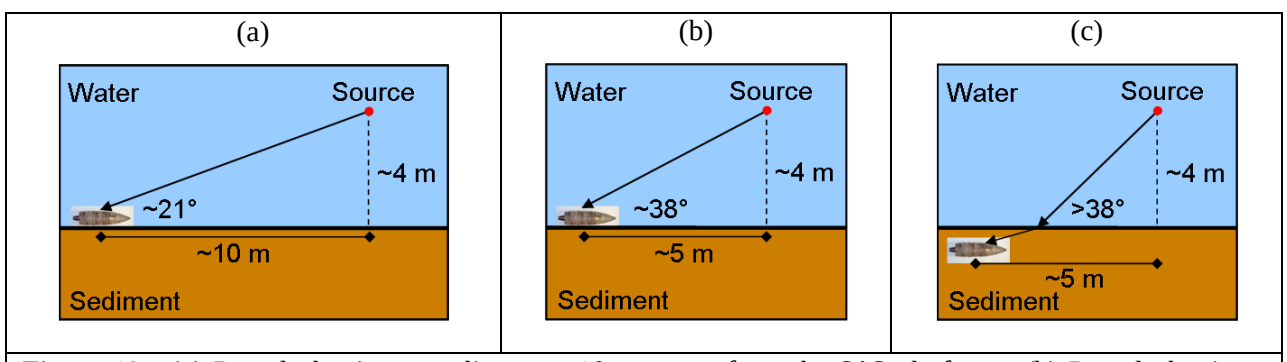

Figure 12. (a) Proud aluminum replica at a 10 m range from the SAS platform. (b) Proud aluminum replica at 5 m range. (c) Flush, buried aluminum target at 5 m range. The local grazing angles at the target for the two ranges are nominally 21° and 38°.

The acoustic templates from the hybrid model and PondEx10 data for the aluminum replica for the geometries of Figure 12 are displayed in Figure 13. The upper row of acoustic templates is the PondEx10 data while the lower row is obtained from the hybrid model. Inspection of Figure 13 demonstrates that the hybrid model captures much of the observed structure found in the PondEx10 data. The differences between model results and data may be caused by a few mechanisms. First, the hybrid model does not contain the affects of surface reverberation. Surface reverberation will decrease the signal-to-noise ratio, and thus, one may anticipate a smearing or broadening of the sharp changes in the target strength. Second, the hybrid model assumed a linear frequency dependence of attenuation over the 1-30 kHz range. Fluid-saturated sand sediments are known to exhibit frequency-dependent dispersion over this frequency range which implies a non-linear frequency dependence of attenuation. The value used in the simulations may therefore be different than that realized in the experiments. In addition, the complex reflection and transmission coefficients at the water-sediment interface are also affected by the choice of attenuation frequency dependence. Third, the burial of the aluminum replica contains some uncertainty in both the depth and orientation. Although the divers measured the depth and tried to place the target with its axis of symmetry parallel to the interface, the effect of any uncertainty in the depth or orientation on the hybrid model results has not been investigated. Finally, the acoustic templates for PondEx10 data are obtained from time windowing the scattered acoustic field, where the incident sound is a 1-30 kHz, 6 ms, LFM chirp while the FE model results are based on plane-wave excitation with essentially infinite duration. The high-Q resonances (e.g., the peaks in the 0-40° range and 7-12 kHz in the hybrid model results) cause a

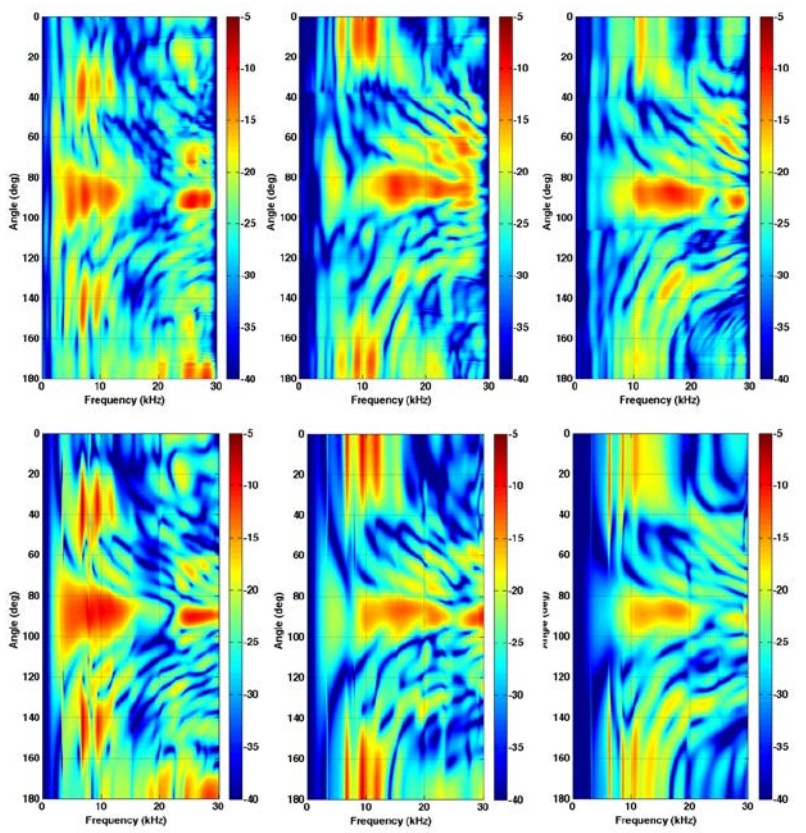

Figure 13. Acoustic templates for different target-in-the-environment scenarios. Left: Proud target at a 10 m range. Center: Proud target at a 5 m range. Right: flush buried target at a 5 m range. The upper row contains PondEx10 data while the lower row depicts the results of FE model simulations.

long-time ring down of a resonantly excited target. The finite-time window, used with the data collection and processing, truncates the ring down, and hence, causes both a reduction in the target strength and a broadening of the peaks.

Figure 14 displays the three narrow band features in the acoustic template of the proud aluminum replica at a 10 m range. Because our hybrid model decomposed the 3D problem of the interaction of an acoustic field with an axisymmetric target into N×2D FE models, where N is the number of azimuthal Fourier modes, the resonances can be associated with a particular mode or modes. The "x" in Figure 14(a) marks a resonance of interest and Figure 14(b) and 14(c) represent the magnitude of the surface displacement of mode 0 and mode 1. Figure 14(d) is the surface displacement when all modes are superposed, and it is clear that mode 1 is the dominant contribution. The arrows in Figure 14(b)-(d) depict the direction of the surface displacement, and inspection of Figure 14(d) shows that the resonance marked by "x" is a bending mode. Finally, the color bar in Figure 14(b)-(d) is a normalized amplitude.

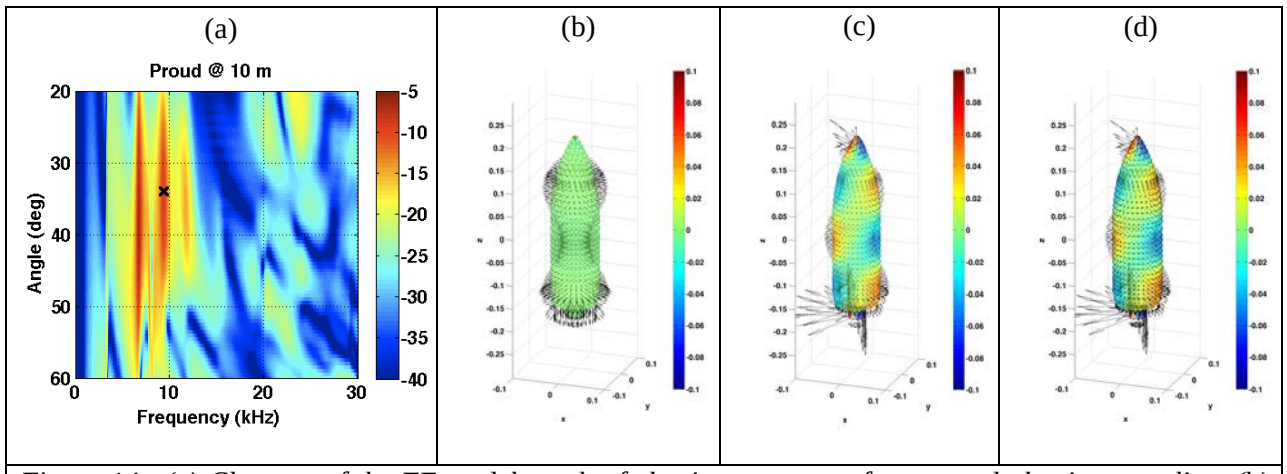

Figure 14. (a) Close-up of the FE model result of elastic resonances for a proud aluminum replica. (b) Surface displacements for mode 0. (c) Surface displacements for mode 1. (d) Superposition of all modes computed by the hybrid model.

The final FE model/PondEx10 data comparison is for a nearly half-buried target, and for our comparison here the target is again the aluminum replica of the bullet-shaped artillery shell. In the PondEx10 experiments, the target was partially buried to between 45 and 50% of its diameter. The range to the target is 10 m with a grazing angle of 21°. The numerical simulation was made possible because of the modal decomposition of the elastic response of the target and the use of an appropriate Green's function in the Helmholtz-Kirchoff propagation integral [10]. The N×2D FE model of a partially buried target is obtained by considering the target to be immersed in water and applying an incident field on the target. The incident field in this case is decomposed numerically on the target surface in azimuthal Fourier modes based on the Fast Fourier Transform (FFT) algorithm. The portion of the target above the water-sediment interface is illuminated by a direct wave and a boundary reflected wave. The portion of the target below the interface is illuminated by an incident wave transmitted into the sediment. The scattered acoustic field is propagated to the receiver via the Helmholtz-Kirchoff integral, where the two-layered fluid medium Green's function is used. Figure 15 displays the acoustic templates for the data/model comparison and comparisons at select aspect angles.

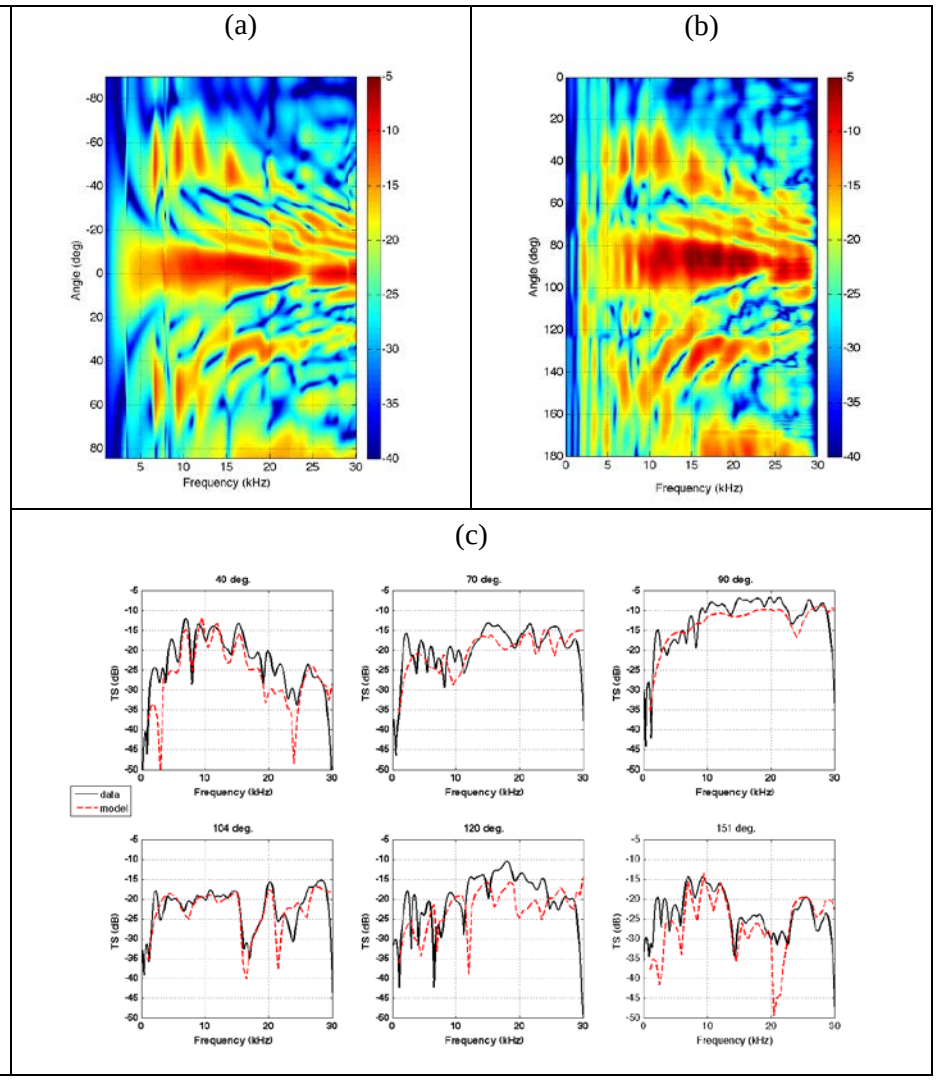

Figure 15. (a) The hybrid model predicted acoustic template for a nearly half-buried aluminum replica of the bullet-shaped artillery shell. (b) Acoustic template for PondEx10 data. (c) Data-model comparison at specific angles. The simulation was performed in a rotated geometry, so an aspect angle of 0° is a broadside orientation of the target while broadside in the experimental geometry is at 90°. The angles listed in (c) are referenced to the angular axis in (b).

Binary Classification: Preliminary Results

In our initial investigation of target discrimination, we considered binary classification (i.e., target-like or not target-like). Two issues that were addressed are: (1) Of the three classifiers available to us, does one perform better than the others; and, (2) How much data is required for proper training of a classifier? Receiver operating characteristic (ROC) graphs were produced for both issues. A ROC graph shows the probability of correctly identifying an object as a target versus identifying a non-target as an target (i.e., a false alarm). The upper left corner of a ROC graph corresponds to correctly classifying all targets as targets with no false alarms. The goal within our preliminary results is not developing new classifiers but to have a classifier-based metric to test how a hybrid model produced acoustic template compares to those derived using experimental-based acoustic templates. The results shown below used methods based on the classification algorithms of Carin and Rabenold [12].

"Virtual experiments" using PondEx10 data were conducted to generate both training feature set data and test feature set data for the nine targets and two rocks. The PondEx10 PCB data from individual targets were used to construct the data sets. A data set was derived from the original data in such a way that clutter (i.e., the rock data) could be added to target data; and thereby, create additional data to test the effects of nearby clutter on the binary classifier. A pass of the APL-UW tower down the rail gives data over about a 40° by 30 kHz region. Acoustic templates for the targets and rocks at a 10 m range were divided into 99 feature matrices [i.e., 11 objects with 9 (40° by 30 kHz) feature matrices per object]. A fast relevance vector machine (RVM) classifier is typically told the number of features that it should identify during training. For 19 features, the RVM identified the feature-bases in Figure 16 (magenta boxes) as the most relevant features for classification.

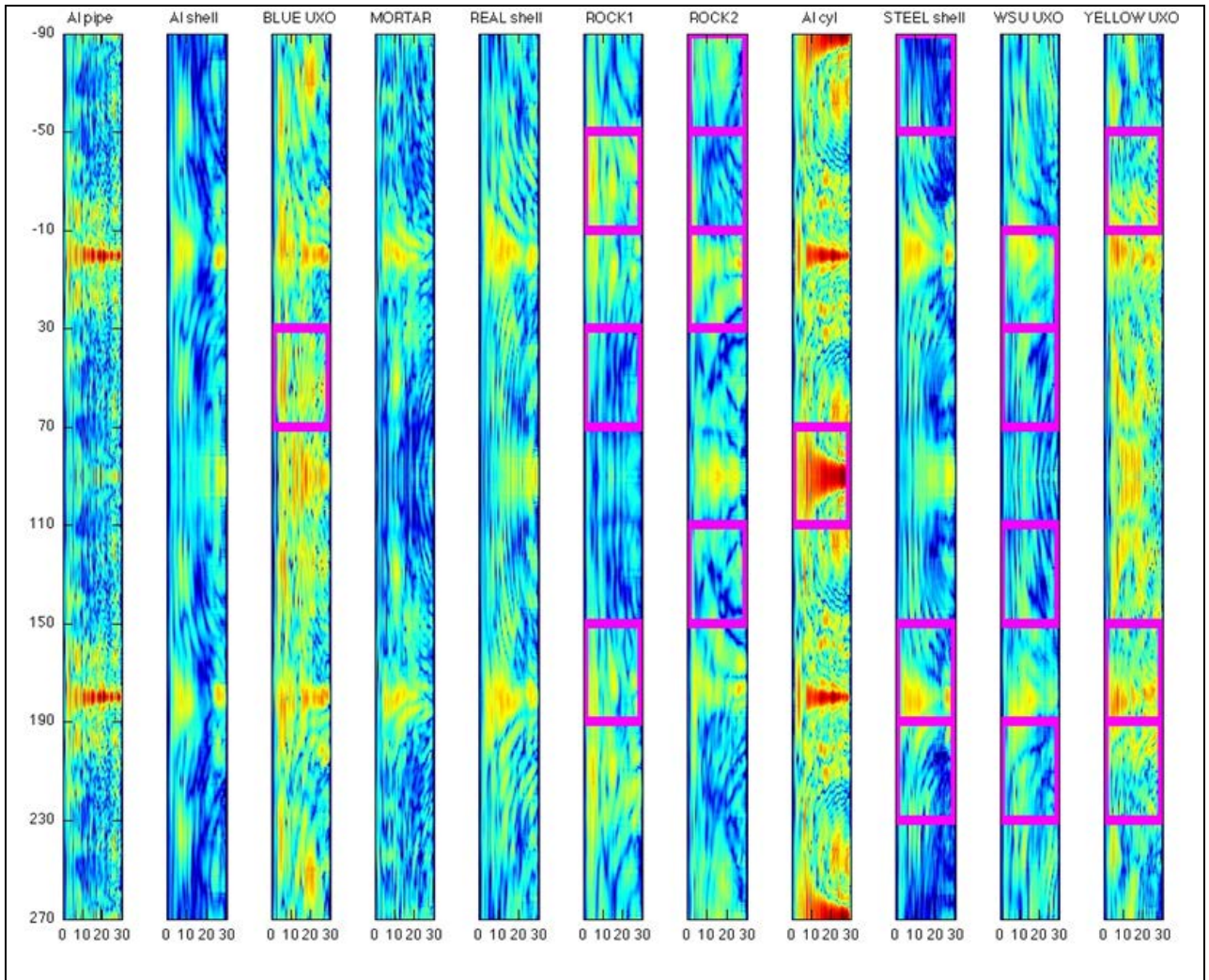

Figure 16. Acoustic templates for the 9 targets and two rocks deployed in PondEx10. The magenta boxes identify 19 feature-bases used by a fast RVM classifier.

The ROC graphs provide the probability of detection versus the probability of false alarm. In the ROC graphs of Figure 17, the binary classification is simply noted as "Correct Class" for correctly detecting a target-like object and a "False Alarm" for all other classifications. The red,

black, and blue lines indicate 33, 19, and 14 feature matrices were used during the training. The first step in using a classifier is training. With the fast RVM algorithm, the use of 33 features may over-train the classifier while using 14 features may under-train the classifier. The ROC curves below suggest that training with 19 features provides satisfactory training of the fast RVM algorithm in this case. (NOTE: of a total of 99 bases were available, typically RVM methods suggest including not more than a fifth of them as features, consistent with what was found in this case).

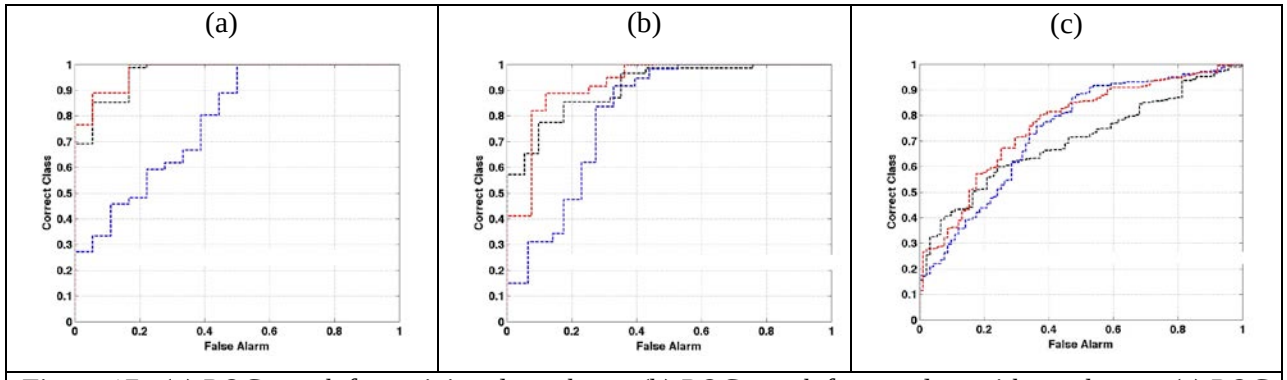

Figure 17. (a) ROC graph for training data alone. (b) ROC graph for test data without clutter. (c) ROC graph for test data with clutter. The number of feature matrices used during training is 33 (red), 19 (black), and 14 (blue).

Prior to completing the investigation of the amount of training data, we also carried out binary classification with three available classifiers: kernel matching pursuit (KMP), support vector machine (SVM), and relevance vector machine (RVM). The schemes again are based on the computational methods of Carin and Rabenold [12]. Training was carried out using 99 bases derived directly from the acoustic templates (of which around 30 features were found to be sufficient for classification), and then testing was performed using 500 virtual experiments with no clutter and 500 virtual experiments including clutter. A testing feature derived from the data is one exemplar made via a random selection from all available PondEx10 data, where target and rock data can be superimposed. For testing feature sets with clutter, the acoustic scattering from a rock was superimposed such that the rock was approximately 1 m in cross-range from the target.

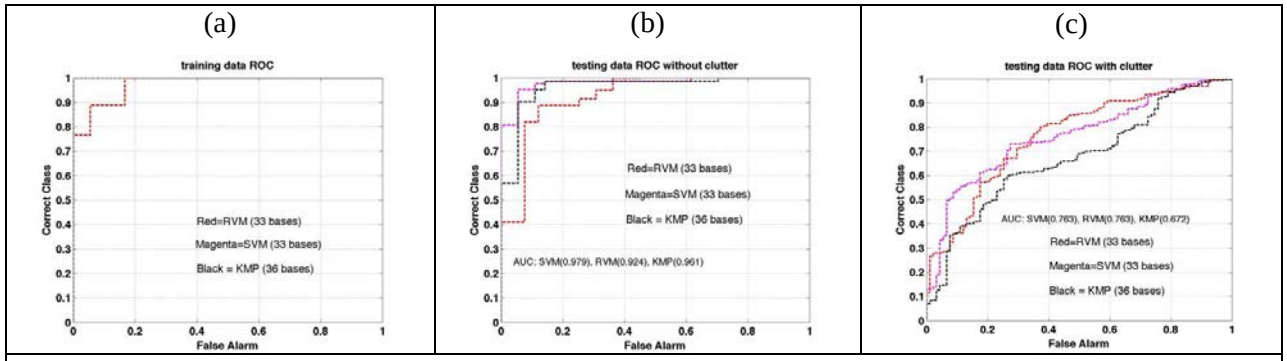

Figure 18. (a) Receiver operating characteristic (ROC) graphs for training data. (b) Test data without clutter. (c) Test data with clutter. The "area under the curve (AUC)" is one metric for the quality of a classifier. While both RVM and SVM classifiers have an AUC of 0.763 when targets are in the presences of clutter, SVM may have a slight advantage if an acceptable false alarm rate cannot exceed ~30%.

Figures 17 and 18 indicate that clutter causes a significant reduction in performance. The classifiers tested with our data are classifiers used with the mine countermeasure community [13] and we treated these as "black boxes". No attempts were made to specifically tune these classifiers to the problem of UXO classification. While some tuning may be possible, it is noteworthy that the SAS filtering algorithm may be an important preconditioning tool, because it can help mitigate the effects of nearby clutter via its spatial windowing.

Conclusion

A central hypothesis running throughout our research is that the environment within which a UXO must be detected and classified alters the acoustic response of the target and the environment must be taken into account in order to develop robust detection and classification strategies. The research conducted under SERDP project MR-1665 took a two prong approach towards resolving issues identified in previous SERDP work that affect sonar detection and classification algorithms of underwater UXO using sonar. The objective was to acquire data on proud, partially buried, and buried munitions over a broad frequency range and aspect angle range and to use these data to develop an inventory of acoustic responses of munitions and to validate propagation and scattering models.

The first prong of our approach involved acoustic scattering measurements from two targets in a quick-look experiment during PondEx09 and then a detailed set of measurements during PondEx10 from nine targets and two rocks of sizes compare to the targets (i.e., clutter). The nine targets included four inert munitions and five scientific targets with well understood elastic responses to an incident acoustic field (see Figures 2 and 3). The measurements were performed in freshwater pond at the NSWC PCD facility 383, which provides a well-controlled yet realistic underwater environment. Physical properties of the environment such as the water's sound speed and the sand sediment's sound speed and attenuation were measured during PondEx09 and PondEx10. The SAS platform deployed for the measurements has been in use since 2002, and it has been shown to provide repeatable acoustic data sets suitable for SAS processing and acoustic template generation in several deployments. Figure 5 is one example of the acquired data (after pulse compression and removal of the baseband from the raw data) and the SAS images formed from the PCB data. Figure 8 displays the set of acoustic templates generated from acoustic data sets for the nine targets and the two rocks, where the objects were in a proud configuration at a 10 m horizontal range. Similar SAS images and acoustic templates for targets at 5 and 10 m horizontal ranges were obtained and reported in the second Interim Report for partially and fully buried targets.

An important outcome of our research established the SAS filtering technique as a method to isolate the scattering signal from closely spaced targets and simultaneously reduce noise due to reverberation. This technique will become more important in an open ocean environment where additional noise components are present (e.g., shipping noise and breaking waves). The technique was applied to all PondEx10 data prior to the construction of any of the acoustic templates presented here.

The second prong to our approach used a hybrid model, which combines a FE model for the elastic response of a target to an incident acoustic field and the Helmholtz-Kirchoff propagation

integral to propagate the target response to a point in space. The hybrid model along with the measured physical properties of the freshwater pond-sand sediment environment was used to predict the acoustic templates for several deployment scenarios. Figure 10 shows the sensitivity of a computed to acoustic template to the fidelity of the FE mesh used in the simulation. Although the acoustic template for smoothed FE mesh case has some agreement with data displayed in Figure 10 the FE mesh that contains the surface structure on the UXO yields better agreement data. The simulations and data for Figure 10 show the inherit trade-off between high-fidelity and the computational complexity. Figure 11 shows that for geometrical identical targets, the material properties of the UXO are important in the coupling acoustic energy to the target and hence the subsequently observed structure in the acoustic template. Although the material used in the fabrication of the real bullet-shaped artillery shell is unknown, its weight and volume suggested that mild steel could be a suitable match. The acoustic templates in Figure 11 clearly demonstrate that in fact a machined replica UXO constructed from mild steel would be a better than a machined replica manufactured from aluminum. To better understand the affect the environment has on the scattering process, the remainder of the acoustic template data/model comparisons used the machined aluminum replica of the real artillery shell and the FE mesh that contained the grooves and ridges. Figure 13 depicts the data/model comparisons for the proud and buried geometries illustrated in Figure 12, and Figure 15 shows the data/model comparison for a partially buried target. In these comparisons, the hybrid-model generated acoustics templates show remarkable agreement with the measured acoustic templates. Figure 14 inspects the underlying modal structure in the elastic response of the machined aluminum replica's acoustic template via hybrid model modal decomposition of the 3D elastic problem into *N* 2D FE problems. This figure shows that the "x"-marked feature in the acoustic template is due to a bending mode the target.

Experimental acoustic templates were used to test three classifiers available to us from the mine countermeasure community. These classifiers are all binary classifiers, where the outcome determines whether an object is target-like or non-target-like. With the limited actual data, "virtual experiments" were conducted where the portion of the PCB data for nine targets and two rocks where superposed to produce new data. This allowed sufficient data for both train and test the classifiers. While the ROC curves in Figures 17 and 18 demonstrate that these classifiers can identity targets from non-target, the curves suggest additional work needs to be performed to understand and reduce the high false alarm rate. It is noted that the classifiers were designed with underwater mine and mine-like objects (i.e., the targets are typically larger than those used in PondEx10) in mind, and we made no attempts at this time to tune the classifiers to UXO other than the standard training procedure.

Acknowledgment

PondEx09 and PondEx10 were conducted under SERDP projects MR-1665 and MR-1666 and with additional support from the Office of Naval Research [Contract N00014-07-G-0557 (Task 0010)]. Dr. Joseph Lopes, Dr. Jermaine Kennedy, and Dr. Raymond Lim from NSWC PCD, and Prof. Philip Marston and Dr. Timothy Marston from Washington State University contributed to PondEx09 and PondEx10 measurements, various aspects of the data analysis, and insights into the structures observed in the SAS images and acoustic templates. The hybrid model predictions were provided by Dr. Aubrey España from APL-UW (ONR Grant N00014-01-1-0394) and Dr. Mario Zampolli from TNO (ONR Global Grant N62909-10-1-7153).

References

[1] TP Long, "A global prospective on underwater munitions," *Mar. Technol. Soc. J.*, **43**, 5-10 (2009).

[2] ML Overfield, LC Symons, "The use of the RUST database to inventory, monitor, and assess risk from Undersea Threats," *Mar. Technol. Soc. J.*, **43**, 33-40 (2009).

[3] A Schwartz, E Brandeburg, "An overview of underwater technologies for operations involving underwater munitions," *Mar. Technol. Soc. J.*, **43**, 62–75 (2009).

[4] JA Bucaro, BH Houston, M Saniga, LR Dragonette, T Yoder, S Dey, L Kraus, L Carin, "Broadband acoustic scattering measurements of underwater unexploded ordnance (UXO)," *J. Acoust. Soc. Am.*, **123**, 738-746 (2008).

[5] KL Williams, SG Kargl, EI Thorsos, DS Burnett, JL Lopes, M Zampolli, PL Marston, "Acoustic scattering from a solid aluminum cylinder in contact with a sand sediment: Measurements, modeling, and interpretation," *J. Acoust. Soc. Am.*, **127**, 3356-3371 (2010).

[6] SG Kargl, KL Williams, TM Marston, JL Kennedy, JL Lopes, "Acoustic response of unexploded ordnance (UXO) and cylindrical targets," *Proc. OCEANS 2010 MTS/IEEE*, Seattle WA, 2010.

[7] TM Marston, KL Williams, PL Marston, "Scattering resonances, filtering with reversible SAS processing, and applications of quantitative ray theory," *Proc. OCEANS 2010 MTS/IEEE*, Seattle WA, 2010.

[8] PT Gough, DW Hawkins, "Unified framework for modern synthetic aperture imaging algorithms," *Int. J. Imaging Syst. Technol.*, **8**, 343-358 (1997).

[9] M Zampolli, A Tesei, FB Jensen, N Malm, JB Blottman, "A computationally efficient finite element model with perfectly matched layers applied to scattering from axially symmetric objects," *J. Acoust. Soc. Am.*, **122**, 1472 (2007).

[10] M Zampolli, A Tesei, G Canepa, OA Godin, "Computing the far field scattered or radiated by objects inside layered fluid media using approximate Green's functions," *J. Acoust. Soc. Am.*, **123**, 4051 (2008).

[11] M Zampolli, AL Espana, KL Williams, SG Kargl, EI Thorsos, JL Lopes, JL Kennedy, PL Marston "Low- to mid-frequency scattering from elastic objects on a sand sea floor: Simulation of frequency and aspect dependent structural echoes", *J. Comp. Acoust.* (Accepted for Publication, June 2012).

[12] L Carin, P Rabenold, Classifier Design for Multi-aspect Low-Frequency Broadband Target Signatures, Technical Report TR-2008/01, ONR contract N00014-06-C-0026.

[13] J Stack, "Automation for underwater mine recognition: current trends and future strategy," *Proc. SPIE - Int. Soc. Opt. Eng*., **8017**, 80170K-1 – 80170K-21, (2011).

[14] SG Kargl, KL Williams, EI Thorsos, JL Lopes, "Bistatic synthetic aperture sonar measurements and preliminary analysis," in *Boundary Influences in High Frequency, Shallow Water Acoustics*, NG Pace and P Blondel (Eds.), University of Bath, UK, Sept., 2005, pp. 137-143.

Appendix A: PondEx09 Data Sets

Orientation (Deg)	Proud 1 - 31 kHz	Proud 30 - 50 kHz	Buried 1 - 31 kHz	Buried 30 - 50 kHz
0	138	139	141	142
20	152	153	155	156
40	158	159	161	162
60	164	165	167	168
80	171	172	174	175
100	178	179	181	182
120	184	185	188	189
140	191	192	194	195
160	198	199	201	202
180	204	205	207	208

Table A1: Data sets for the bullet-shaped artillery shell in target field. The orientation of the shell with respect to the APL-UW rail system is listed in the first column and the exposure state is given in the remaining columns.

Orientation (Deg)	Proud 1 - 31 kHz	Proud 30 - 50 kHz	Buried 1 - 31 kHz	Buried 30 - 50 kHz
0	217	218	220	221
20	223	224	227	228
40	230	231	233	234
60	238	239	241	242
80	245	246	248	249
100	255	256	258	259
120	262	263	265	266
140	269	270	272	273
160	276	277	279	280
180	283	284	286,288	287

Table A2: Data sets for an 81-mm mortar at a 10 m range in target field. The orientation of the mortar with respect to the APL-UW rail system is listed in the first column.

Appendix B: PondEx10 Data Sets

Table B1 enumerates the data sets collected with five targets in the field at a 10 m horizontal range. The targets located in TP1 through TP5 are a machined aluminum replica, 2:1 solid aluminum cylinder, machined steel replica, 2:1 aluminum pipe, and bullet-shaped artillery shell, respectively. The first column corresponds to the mobile tower moving left-to-right on the rail system with the source transmitting a 1-31 kHz LFM chirp. Column two corresponds to the right-to-left motion of the mobile tower, where the source transmitted a 30-50 kHz LFM chirp. "APL" in Table B1 denotes the sequence number assigned by APL to a monostatic SAS data set recorded on APL's mobile tower. The two character mnemonic is the sequence "number" used by NSWC PCD for the bistatic data sets collected by the stationary tower. The NSWC PCD sequence numbers are included to allow for the ease of cross referencing between the APL and NSWC PCD data sets. The last column is the rotation angle of the targets with respect to the APL-UW rail system.

1 - 30 kHz		30 - 50 kHz		Angle	1 - 30 kHz		30 - 50 kHz		Angle
APL	NSWC	APL	NSWC	(Deg)	APL	NSWC	APL	NSWC	(Deg)
27	AI	28	AJ	0	37	AS	38	AT	80
29	AK	30	AL	10	39	AU	40	AV	-20
31	AM	32	AN	20	41	AW	42	AX	-40
33	AO	34	AP	40	43	AY	44	AZ	-60
35	AQ	36	AR	60	45	BA		BB	-80

Table B1: Data sets for five proud targets in the 10 m target field. The data set at ~10° was an incorrect target alignment, which was caused by the divers' initial experience with the new alignment frame.

Table B2 enumerates the data sets collected with seven targets in the field at a 10 m horizontal range. The targets located in TP1 through TP5 are Rock 1, 2:1 solid aluminum cylinder, machined steel replica, 2:1 aluminum pipe, and rock 2. The machined aluminum replica was placed between TP2 and TP3 and the bullet-shaped artillery shell was placed between TP3 and TP4. The separation distance between a rock and its adjacent target is 3 m while the separation distance between the other targets is 1.5 m. Due to the asymmetry of the rocks, these targets were rotated through a larger angular range. For the data sets 100° to 180° only the rocks were rotated and the other targets remained at an 80° orientation. After the measurements up to 180° were completed, the targets were removed and other scheduled experiments were conducted. The asymmetry of the rocks required additional angular rotations to cover the entire 360° range. Rocks 1 and 2 were placed in TP1 and TP2, respectively, and no other targets are present. The sequence numbers 433 to 447 were then recorded. Finally, bistatic data were not collected during this final set of rotation measurements.

1 - 30 kHz		30 - 50 kHz		Angle	1 - 30 kHz		30 - 50 kHz		Angle
APL	NSWC	APL	NSWC	(Deg)	APL	NSWC	APL	NSWC	(Deg)
47	BC	48	BD	-80	66	BV			120†
49	BE	50	BF	-60	67	BW			140†
51	BG	52	BH	-40	68	BX			160†
53	BI	54	BJ	-20	69	BY			180†
55	BK	56	BL	0	433		434		200‡
57	BM	58	BN	20	436		438		220‡
59	BO	60	BP	40	440		441		240‡
61	BQ	62	BR	60	443		444		260‡
63	BS	64	BT	80	446		447		280‡
65	BU			100†					

Table B2: Data sets for seven proud targets in the 10 m target field.
† Only the rocks were rotated.
‡ Final set of rotations for the rocks.

Williams *et al* noted that the scattering for a proud target may be dependent on the phase of the reflection coefficient at the water-sediment interface [5]. To remove this sensitivity from several sets of measurements, two plexiglass plates were placed in TP4 and TP5. The reflection coefficient of plexiglass is well-known and not subject to variation. These plates had octagonal shapes, because the corners were removed to prevent scattering from the 90° corners. Initially, the 2:1 solid aluminum cylinder and aluminum pipe were used as reference targets. The sequence numbers for data recorded at various rotation angles are listed in Table B3. The first entry is a background from the plates alone (which would permit background subtraction of any scattering from the plates). In these initial measurements, an edge of the plates was aligned parallel to the rail system, and it produced a strong feature in the SAS images. The scattering from the edge is not easily removed from the baseband pulse-compressed time signals, so the plates were rotated by 22°, which points a corner of the octagon at the rail system. The sequence numbers for a second set of measurements after the plate rotation are given in Table B4.

1 - 30 kHz		30 - 50 kHz		Angle	1 - 30 kHz		30 - 50 kHz		Angle
APL	NSWC	APL	NSWC	(Deg)	APL	NSWC	APL	NSWC	(Deg)
74	CB	75	CC	†	80	CH	81	CI	40
76	CD	77	CE	0	82	CJ	83	CK	60
78	CF	79	CG	20	84	CL	85	CM	80

Table B3: Data sets for the 2:1 solid aluminum cylinder and pipe on plexiglass plates.
† No targets were on the plates for a background data set.

1 - 30 kHz		30 - 50 kHz		Angle	1 - 30 kHz		30 - 50 kHz		Angle
APL	NSWC	APL	NSWC	(Deg)	APL	NSWC	APL	NSWC	(Deg)
86	CN	87	CO	†	92	CT	93	CU	40
88	CP	89	CQ	0	94	CV	95	CW	60
90	CR	91	CS	20	96	CX	97	CY	80

Table B4: Data sets for 2:1 solid aluminum cylinder and pipe on plexiglass plates. Plates rotated 22° to suppress glint from edge scattering.
† No targets were on the plates for a background data set.

Once the data sets from the reference targets were collected, the aluminum cylinder and pipe were replaced by the machined aluminum replica in TP4 and by the machined steel replica in TP5. The data sets are listed in Table B5. With the known reflection coefficient for the plexiglass and the identical target shapes, these measurements allow one to investigate the importance of an elastic response from the targets. These data sets, combined with on-going FE modeling of the target response, should yield an unambiguous understanding of the scattering from this particular target shape.

1 - 30 kHz		30 - 50 kHz		Angle	1 - 30 kHz		30 - 50 kHz		Angle
APL	NSWC	APL	NSWC	(Deg)	APL	NSWC	APL	NSWC	(Deg)
98	CZ	99	DA	0	111	DJ	112	DK	-20
100	DB	101	DC	20	113	DL	114	DM	-40
102	DD	103	DE	40	117	DN	118	DO	-60
104	DF	105	DG	60	119	DP	120	DQ	-80
106	DH	107	DI	80					

Table B5: Data sets for machined aluminum replica and machined steel replica on plexiglass plates. Plates rotated 22° to suppress glint from edge scattering.

A series of measurements were conducted with a 152-mm TP-T round, small aluminum cylinder with a notch, the steel artillery shell, an 81-mm mortar, and the machined aluminum replica. Tables B6, B7, and B8 list the sequence numbers for the measurements that were conducted for proud targets, “half-buried” targets, and fully buried targets, respectively.

1 - 30 kHz		30 - 50 kHz		Angle	1 - 30 kHz		30 - 50 kHz		Angle
APL	NSWC	APL	NSWC	(Deg)	APL	NSWC	APL	NSWC	(Deg)
185	EH	186	EI	0†	195	ER	196	ES	0
187	EJ	188	EK	-80	197	ET	198	EU	20
189	EL	190	EM	-60	199	EV	200	EW	40
191	EN	192	EO	-40	201	EX	202	EY	60
193	EP	194	EQ	-20	203	EZ	204	FA	80

Table B6: Data sets for the following five proud targets at a 10 m range: small aluminum cylinder with a notch, 152 mm TP-T round, steel artillery shell, 81 mm mortar, and machined aluminum replica.
† Initial data set was used to check the source level and required compensation by a factor of 2.

1–30 kHz		30–50 kHz		Angle	1–30 kHz		30–50 kHz		Angle
APL	NSWC	APL	NSWC	(Deg)	APL	NSWC	APL	NSWC	(Deg)
205	FB	206	FC	-80	215	FL	216	FM	20
207	FD	208	FE	-60	217	FN	218	FO	40
209	FF	210	FG	-40	219	FP	220	FQ	60
211	FH	212	FI	-20	221	FR	222	FS	80
213	FJ	214	FK	0					

Table B7: Data sets for the following five "half-buried" targets at a 10 m range: small aluminum cylinder with a notch, 152-mm TP-T round, bullet-shaped artillery shell, 81-mm mortar, and machined aluminum replica.

1 - 30 kHz		30 - 50 kHz		Angle	1 - 30 kHz		30 - 50 kHz		Angle
APL	NSWC	APL	NSWC	(Deg)	APL	NSWC	APL	NSWC	(Deg)
223	FT	224	FU	0	233	GD	234	GE	80
225	FV	226	FW	-20	235	GF	236	GG	-40
227	FX	228	FY	20	237	GH	238	GI	-60
229	FZ	230	GA	40	239	GJ	240	GK	-80
231	GB	232	GC	60					

Table B8: Data sets for the following five fully-buried targets at a 10 m range: small aluminum cylinder with notch, 152-mm TP-T round, bullet-shaped artillery shell, 81-mm mortar, and machined aluminum replica.

After the data in Tables B6, B7, and B8 were collected, the targets were removed from the target field and other scheduled measurements were carried out. Upon acquisition of the 155-mm howitzer projectile, a new target field was prepared by the divers at the 10 m range. The light blue areas in Figure 4 were filled with sand and the divers flattened these areas and the target patches with hand trowels. The divers also removed a berm that accumulated at the rear of the target field. Six targets were deployed with the 152-mm TP-T round in TP2, the bullet-shaped artillery shell in TP3, an 81-mm mortar in TP4, the 155-mm howitzer projectile in TP5, the small aluminum cylinder with a notch between TP2 and TP3, and the machined aluminum replica between TP3 and TP4. The separation distance between adjacent targets is 1.5 m. Tables B9, B10, and B11 list the sequence numbers for the measurements that were conducted for proud targets, "half-buried" targets, and fully-buried targets, respectively.

Tables B12 and B13 contain the data sequence numbers for experiments conducted in a target field that was 5 m from the rail system. The target field at 5 m was prepared by the divers in the same manner as the 10 m target field. These measurements augment those conducted during PondEx09 at a 40° grazing angle for proud and fully-buried targets. During PondEx09, neither the 152-mm TP-T round, the-155 mm howitzer projectile, nor machined aluminum replica were available.

1 - 30 kHz		30 - 50 kHz		Angle	1 - 30 kHz		30 - 50 kHz		Angle
APL	NSWC	APL	NSWC	(Deg)	APL	NSWC	APL	NSWC	(Deg)
241	GL	242	GM	†	253	GX	254	GY	0
243	GN	244	GO	†	255	GZ	256	HA	20
245	GP	246	GQ	-80	257	HB	258	HC	40
247	GR	248	GS	-60	259	HD	260	HE	60
249	GT	250	GU	-40	261	HF	262	HG	80
251	GV	252	GW	-20					

Table B9: Data sets for the following six proud targets at a 10 m range: 152-mm TP-T round, bullet-shaped artillery shell, 81-mm mortar, 155-mm howitzer projectile, small aluminum cylinder with a notch between TP2 and TP3, and the machined aluminum replica between TP3 and TP4.
† Background run.

1–30 kHz		30–50 kHz		Angle	1–30 kHz		30–50 kHz		Angle
APL	NSWC	APL	NSWC	(Deg)	APL	NSWC	APL	NSWC	(Deg)
263	HH	264	HI	80	273	HR	274	HS	0
265	HJ	266	HK	60	275	HT	276	HU	-20
267	HL	268	HM	40	277	HV	278	HW	-40
269	HN	270	HO	20	279	HX	280	HY	-60
271	HP	272	HQ	0	281	HZ	282	IA	-80†

Table B10: Data sets for the following six "half-buried" targets at a 10 m range: 152-mm TP-T round, bullet-shaped artillery shell, 81-mm mortar, 155-mm howitzer projectile, small aluminum cylinder with a notch between TP2 and TP3, and the machined aluminum replica between TP3 and TP4.
† Targets settled overnight in field.

1–30 kHz		30–50 kHz		Angle	1–30 kHz		30–50 kHz		Angle
APL	NSWC	APL	NSWC	(Deg)	APL	NSWC	APL	NSWC	(Deg)
283	IB	284	IC	-80	293	IL	294	IM	0†
285	ID	286	IE	-60	295	IN	296	IO	20
287	IF	288	IG	-40	297	IP	298	IQ	40
289	IH	290	II	-20	299	IR	300	IS	60
291	IJ	292	IK	0	301	IT	302	IU	80

Table B11: Data sets for the following six fully-buried targets at a 10 m range: 152-mm TP-T round, steel artillery shell, 81-mm mortar, 155-mm howitzer projectile, small aluminum cylinder with a notch between TP2 and TP3, and the machined aluminum replica between TP3 and TP4.
† Targets settled over Sunday.

1 - 30 kHz		30 - 50 kHz		Angle	1 - 30 kHz		30 - 50 kHz		Angle
APL	NSWC	APL	NSWC	(Deg)	APL	NSWC	APL	NSWC	(Deg)
363*		364*			365†	JU	366†	JV	
367	JW	368	JX	-80	379	KI	380	KJ	20
369	JY	370	JZ	-60	381‡	KK	382	KL	40
371	KA	372	KB	-60	383	KM	384	KN	40
373	KC	372	KD	-40	385	KO	386	KP	60
375	KE	376	KF	-20	387	KQ	388	KR	80
377	LG	378	LH	0					

Table B12: Data sets for the following five proud targets at a 5 m range: small aluminum cylinder with a notch, 152 mm TP-T round, machined aluminum replica, 81 mm mortar, 155 mm howitzer projectile.
** Target field was not smoothed, and the 152 mm TP-T round was in TP3.*
† Background run after the divers prepared the target field.
‡ Data set contains 5 second of dead time at ping 400.

1 - 30 kHz		30 - 50 kHz		Angle	1 - 30 kHz		30 - 50 kHz		Angle
APL	NSWC	APL	NSWC	(Deg)	APL	NSWC	APL	NSWC	(Deg)
391	KU	392	KV	60	399	LC	400	LD	-20
393	KW	394	KX	40	401	LE	402	LF	-40
395	KY	396	KZ	20	403	LG	404	LH	-60
397	LA	398	LB	0	405	LI	406	LJ	-80

Table B13: Data sets for the following five fully-buried targets at a 5 m range: small aluminum cylinder with a notch, 152-mm TP-T round, machined aluminum replica, 81-mm mortar, 155-mm howitzer projectile.